work in progress

Bias-Variance Trade-Off in *In Vivo* Metabolite Quantitation

D. van Ormondt, R. de Beer
Applied Physics, TU Delft, NL

J.W.C. van der Veen
MRS Core Facility
NIMH, NIH, Bethesda, USA

D.M. Sima
ESAT-SCD
KU Leuven, BE

D. Graveron-Demilly
CREATIS-LRMN, Univ Lyon 1
CNRS UMR 5220
INSERM U1044, INSA
Lyon, FR

***Abstract*—In *in vivo* metabolite quantitation, the model function of the attendant MRS signal is often only partly known. This unfavourable condition requires semi-parametric estimation. In the present study the unknown part is the form of the decay function of the signal. The lack of knowledge is caused by micro-heterogeneity of the tissue hosting the metabolites. At high magnetic field, *i.e.*, ≥ 10 Tesla, it seems reasonable to assume the decay function to be independent of the metabolite species. This assumption enabled us to circumvent the often cumbersome search in *function* space, normally required in semi-parametric estimation. We investigated the favourable consequences of this simplification for bias-variance trade-off.**

***Index Terms* — metabolite quantitation, micro-susceptibility, signal-decay function, semi-parametric, bias-variance trade-off**

I. Introduction

In vivo Magnetic Resonance Spectroscopy (MRS) is the sole method capable of measuring concentrations of markers of disease – metabolites – on arbitrary locations inside patients, non-invasively; see. *e.g.*, [1]. Metabolite concentrations are estimated from an MRS-signal by fitting to it an appropriate model function. Given the unique property of MRS, it is of paramount importance to reduce the errors of estimation as much as possible.

A perennial problem is that parts of the MRS model function are unavoidably unknown. Fitting a known model function to data amounts to a search in *parameter* space. This is relatively easy, including prediction of estimation errors. On the other hand, fitting a partly unknown model function to data involves a search in *function* space too which is cumbersome by comparison, not in the least with respect to prediction of estimation errors [2].

Combination of parameter estimation and function estimation is called semi-parametric estimation [3], [4]. It is the only way of fitting incomplete model functions to data. Unavoidably, it results in biased estimates of the parameters of the known part of the model function.

This report concerns bias-variance trade-off in semi-parametric estimation of metabolite concentrations from *in vivo* MRS signals. *In vivo* MRS signals are measured in the time-domain. In the present study, the unknown part of the model function is the form of the decay of the *in vivo* MRS signal as a function of time. The condition is caused by unknown inhomogeneity on spatial micro-scale of the magnetic field within a patient due to micro-susceptibility effects [5], [6].[1]

Estimation errors are obtained from a Monte Carlo simulation, using thousand different noise realisations with equal mean and equal standard deviation.

II. Methods

A. Model function

An *in vivo* MRS signal, $s(t)$, is complex-valued and is acquired in the time-domain; see, *e.g.*, [7]. Apart from noise it can be modelled by

$$s(t) = e^{\imath\varphi_0} \sum_{m=1}^{M} c_m \, d_m(t) \, s_m(t) \, e^{\imath\,(2\pi\triangle\nu_m t + \varphi_m)} \,, \qquad (1)$$

in which $\imath = \sqrt{(-1)}$, φ_0 is an overall phase, φ_m is a metabolite-dependent phase, $t = n\triangle t + t_0$ is time, with $\triangle t$ is the sampling interval, $n = 0, 1, \ldots, N-1$, t_0 a 'dead' time put to zero in this study, and $m = 1, \ldots, M$ are the indexes of the metabolites. Furthermore:

- c_m is the amount or concentration of metabolite m; it is the most important piece of information for clinicians.
- $d_m(t)$ governs the decay of the signal of metabolite m. In *in vivo* measurements, the form of $d_m(t)$ is *a priori* unknown due to heterogeneity of living objects.
  - In Sec. II-B, we approximate the decay by the surrogate model function $d_m(t) = e^{\alpha_m t}$ with $\alpha_m < 0$, following an often applied, accepted nonlinear least-squares fit procedure; see, *e.g.*, [7].
  - In Sec. II-C, we apply an alternative, new method: The decay is approximated by an expression that depends on the – initially unknown – concentrations $c_m, m = 1, \ldots M$. Incorrectness of substituted c_m values perturbs the form of the expression in a particular, easily discernible way [8], [9]. However, once the c_m are correct, the perturbation disappears,

[1] Note that partial ignorance about all effects that possibly contribute to any measured data is the rule rather the exception.

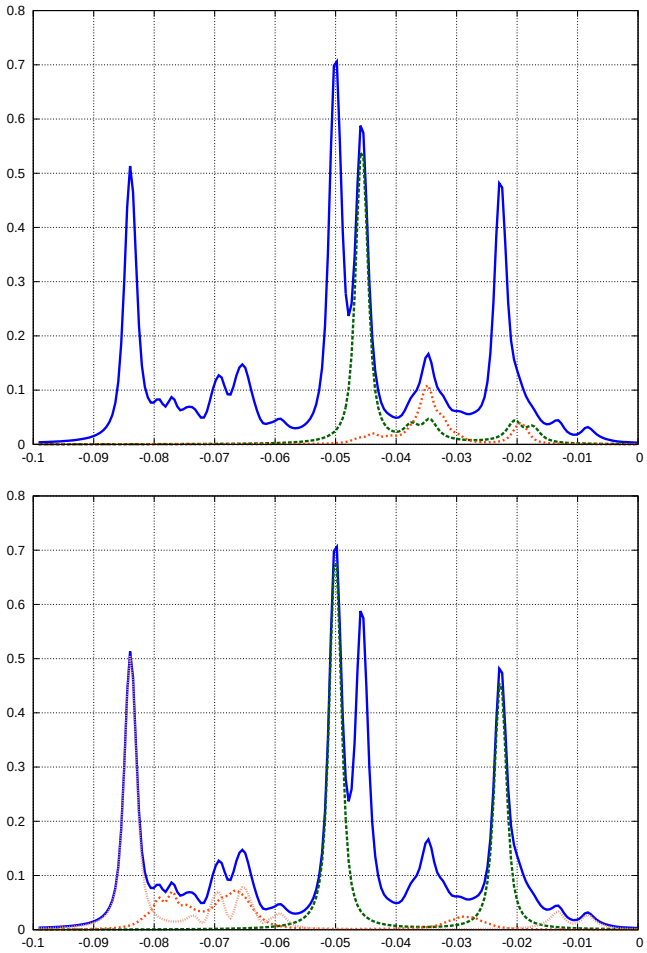


Figure 1. Real part of the FFT (spectrum) of a noiseless MRS-signal (blue) simulated with Eq. (1) in combination with $d_m(t) = d(t) = \exp(\alpha t + \beta t^2); \alpha, \beta < 0$. Also shown are the separate spectra of the five contributing metabolites. Upper: Metabolites 1,4; green: Choline, red: Myo inositol. Lower: Metabolites 2,3,5; green: Creatine, red: Glutamate, brown: N-acetylaspartate. Horizontal axis: Frequency region where the metabolite spectrum is located, the total region stretching from -0.5 (left) to +0.5 (right). NB. Here, we do not adhere to the confusing MRS-practice of reversing the sign of the horizontal axis. Vertical axis: Intensity in arbitrary units. $B = 3$ Tesla.

similar to the vanishing residue of a least-squares fit. We exploit this property to estimate the correct, true values of the c_m. The complete form of $d_m(t)$ remains unknown but this of no concern to clinicians.

- $s_m(t) = \sum_{k=1}^{K_m} a_{m,k}\ e^{\imath\,(2\pi\nu_{m,k}t + \varphi_{m,k})}$ is the *a priori* known, non-decaying version of the model function of metabolite m, in which $a_{m,k}, \nu_{m,k}, \varphi_{m,k}$ are the relative amplitudes, frequencies, and phases of individual spectral components[2] of a metabolite model function. The signals $s_m(t)$ used in this study were calculated with the software package NMRSCOPE [10] which is part of the metabolite quantitation software package jMRUI [7].
- $\triangle\nu_m, \varphi_m$ are unknown shifts of the overall frequency and overall phase of $s_m(t)$ due to experimental conditions.

[2]Spectral component: *e.g.*, $e^{\imath\,(2\pi\nu_{m,k}t + \varphi_{m,k})}$, also called sinusoid. Spectral line: 'peak' in a spectrum, *i.e.*, FFT of a sinusoid.

In the present work, a simulated MRS-signal containing contributions from five metabolites is used; see [9]. Fig.1 shows the FFT (spectrum) of the signal including the FFT's of the contributing metabolites. The signal was simulated with Eq. (1), substituting $d_m(t) = e^{\alpha t + \beta t^2}, \alpha, \beta < 0$. Note the extra, quadratic term in the exponent. When estimating parameters from the simulated signal we assume ignorance about its existence. The task is to fit the model function of Eq. (1) to noisy versions of the simulated MRS-signal by varying the values of the unknown physical model parameters. In Sec. II-B, fitting is done with a gradient search, using the surrogate analytic model function $d_m(t) = e^{\alpha t}$, *i.e.*, putting $\beta = 0$, thus mimicking ignorance about the true form of the decay. In Sec. II-C correct parameters c_m are searched for with a genetic algorithm concentrating on only a detail of the decay.

B. Method 1. Surrogate analytic decay function

Fitting an analytic model function by nonlinear least-squares (NLLS) is a standard technique [11]. We fit the model function of Eq. (1) using $d_m(t) = e^{\alpha_m t}$, $\alpha_m < 0$, to a signal simulated with Eq. (1) using $d_m(t) = d(t) = e^{\alpha t + \beta t^2}, \alpha, \beta < 0$.
In this report, the parameters to be fitted were φ_0 and $c_m,\ \alpha_m, \triangle\nu_m, m = 1, \ldots, M$. The remaining parameters in Eq. (1) were assumed known. From here on, we indicate this fit procedure by method 1.
Because the fit was made intentionally with $\beta = 0$ while in the signal $\beta \neq 0$, the resulting estimates became biased. In addition, statistical errors were incurred when random noise was added to the signal.
To obtain the relative magnitudes of the bias and standard deviation we performed the following simple Monte Carlo simulation. First, the noiseless simulated signal was corrupted with thousand different random noise signals, each having the same mean and standard deviation. Subsequently, each noise-corrupted signal was subjected to the NLLS-fit mentioned above. This yielded thousand different values of each estimated parameter. Since in a simulation the true value of each parameter is known, both bias and standard deviation could be computed.
In order to study the influence of the noise level on the bias-to-standard deviation ratio, the mentioned procedure was repeated for seven different noise levels, starting at noise = zero.

C. Method 2. Experimental decay function

Physical conditions: In the previous Section, an incorrect yet convenient analytic model function — Eq. (1) with $d_m(t) = e^{\alpha_m t}$ — was fitted to the signal. An important advantage of this approach is that the attendant NLLS-fitting is reliable and quick. An important drawback is that the resulting parameter estimates are biased in principle. In the present Section we attempt to avoid bias through a very different approach. Key physical considerations in the approach are

(a) The form of the decay is determined by micro-susceptibility in the volume of interest [5], [8].

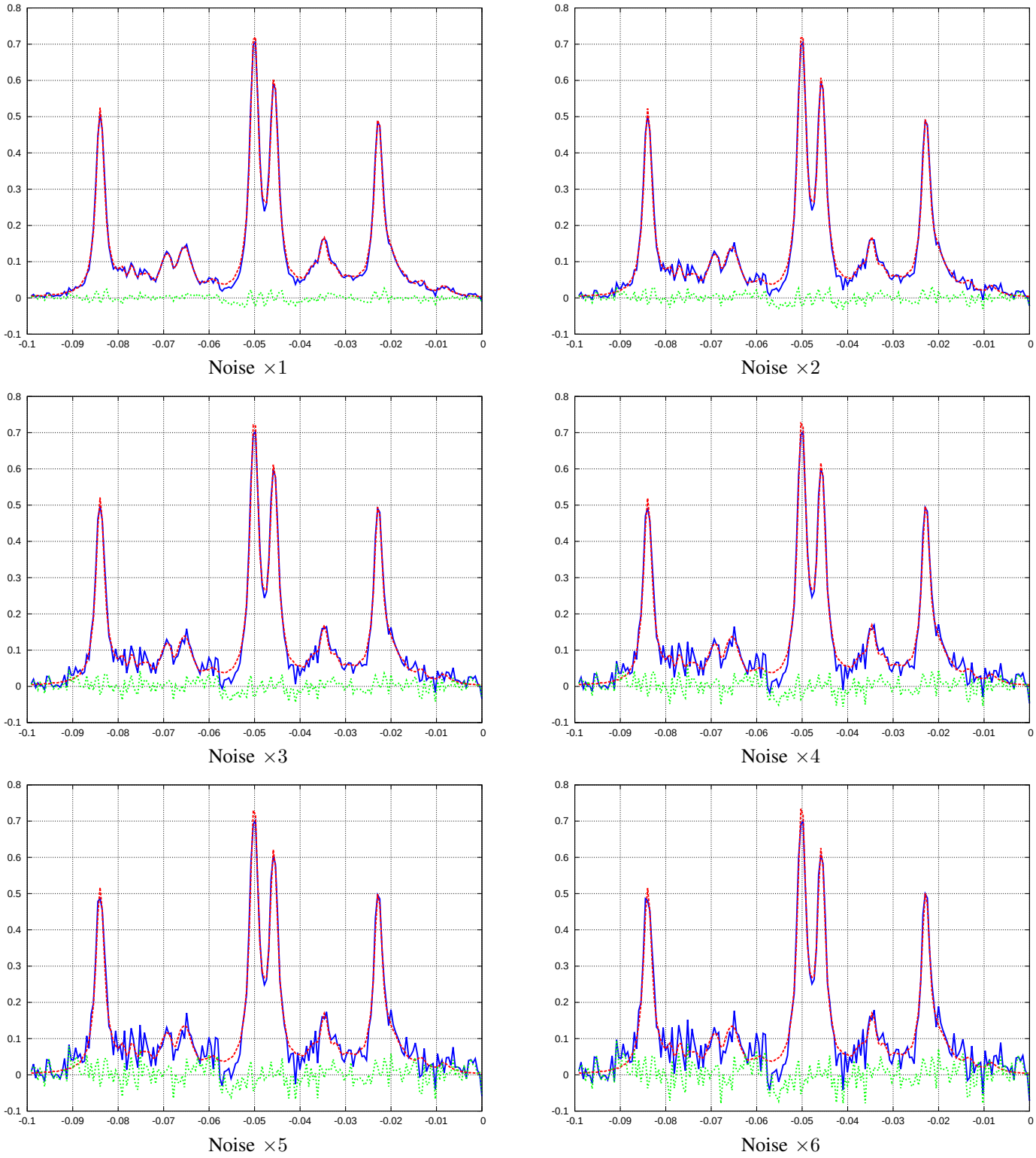


Figure 2. Real part of the FFT of the fit of a model function – called spectrum – with exponential decay for six levels of the SNR (Noise $\times 1, \times 2, \times 3, \times 4, \times 5, \times 6$) to a signal with an additional, Gaussian decay. For these plots, the angle φ_0 in Eq. (1) was put to zero. Blue: Signal. Red: Fitted model function. Green: Residue. Horizontal axis: Frequency region where the metabolite spectrum is located; the total spectral region is from -0.5 to +0.5. Vertical axis: Intensity in arbitrary units. At high SNR, upper left, the residue of each of the four singlets, at $\nu \approx -0.084, -0.050, -0.046, -0.022$ can be seen to contain a doublet. This doublet shape originates from the difference between exponential and Gaussian decay. With decreasing SNR the doublets gradually disappear into the random noise.

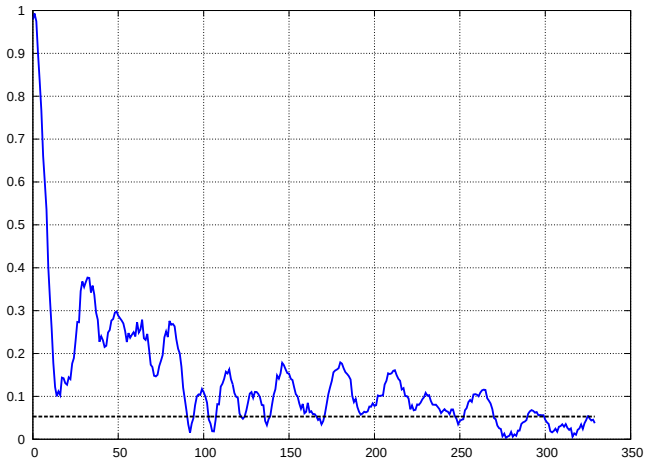


Figure 3. $|s(t_n)|$ corresponding to Fig. 2, 'Noise ×3', left side, middle. Horizontal axis: t_n, in units of $\triangle t$. The horizontal, black, dashed line is at $|s(t_n)| = 2.5 \times \sigma_{noise}$, causing omission of sample points n = 92-95, 104-108, 123-124, 137-139, 168-171, 249-253, 271-290, 301-325, 327-329, *i.e.*, excluded from selection in the argument of Eq (4), below.

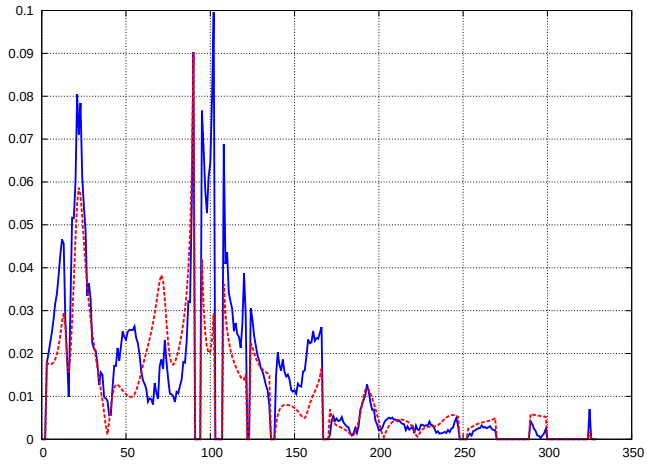


Figure 4. Plot of $\left| d(t_n)^{\mathrm{expm,post_pikaia}}_{\mathrm{highpassed}} - d(t_n)^{\mathrm{expm,pre_pikaia}}_{\mathrm{highpassed}} \right|$, showing the effect of Eq. (4). Horizontal axis: t_n, in units of $\triangle t$. The superscripts 'post-pikaia' and 'pre-pikaia' relate to respectively the situation *after* and *before* executing Eq. (4), for two cases: Blue, noise in $s(t_n)$ is as shown in Fig. 2, 'Noise ×3', left side, middle. Red, noise in $s(t_n)$ is zero, included for referencing. Omission of sampling points corresponds to Fig. 3. The effect of Eq. (4) in both the noisy and noiseless case is clearly visible.

(b) Given point (a), it seems plausible that the decay is the same for all sinusoids in the signal. This conjecture is still under investigation.

(c) Spectral lines (*i.e.*, FFT of sinusoid) in MRS-spectra are narrow, implying that the decay of the sinusoids in the signal is slow.

Estimation steps: Exploiting the physical conditions described above, we devised an estimation method comprising the following three steps.

(1) Get starting values.
As in Sec. II-B, Eq. (1) with $d_m(t) = e^{\alpha_m t}$ is fitted to signal. The resulting c_m and α_m are biased, but we assumed that the frequency shifts $\triangle\nu_m$ were estimated correctly. In the sequel, only the c_m are further improved. The α_m are no longer needed. The $\triangle\nu_m$ are fixed to the values obtained in this first step.

(2) Compute an experimental decay function
Using the above point (b), one can rewrite Eq. (1) as

$$s(t) = d(t)\, e^{\imath\varphi_0} \sum_{m=1}^{M} c_m\, e^{\imath\, 2\pi\triangle\nu_m\, t}\, s_m(t)\ , \qquad (2)$$

and from this an 'experimental' model function for $d(t)$,

$$d(t)^{\mathrm{expm}} = \frac{s(t)}{e^{\imath\varphi_0} \sum_{m=1}^{M} c_m\, e^{\imath\, 2\pi\triangle\nu_m\, t}\, s_m(t)}\ , \qquad (3)$$

which depends on physical model parameters only. In absence of measurement noise and given the true values of the model parameters in the denominator, Eq. (3) yields the true decay. However, measurement noise and suboptimality of the parameter values obtained in the previous step distort the result. See [8], [9], [12] for various typical distortions of $d(t)^{\mathrm{expm}}$.
A new approach in the present work is reduction of the noise in the numerator of Eq. (3) *prior to executing the division*, using the State-Space based method HSVD [13]. The rationale of this approach is that the original Gaussian probability distribution of measurement noise is distorted during the division, making it rather less tractable.

Two alternative ways exist to proceed to step (3):

(3) Search in function space or in parameter space

i. **Search in function space.**
The NLLS-fit of Eq. (1) to the data can be improved by replacing the approximate function $d(t) = e^{\alpha t}$ with the experimental decay function $d(t)^{\mathrm{expm}}$. To really make this work, the distortion of $d(t)^{\mathrm{expm}}$ is to be smoothed. The latter is achieved by a search in *function* space with the aid of splines or other functions like, *e.g.*, wavelets; see [12] and references therein. This procedure can be iterated several times, resulting in better physical model parameters and a better decay function. A stop criterion is attaining a minimal residue of the NLLS-fit. Coincidence of this criterion with obtaining the optimal physical parameter values is not guaranteed though. This is the universal dilemma of semi-parametric estimation.

ii. **Search in parameter space.**
Instead of improving the NLLS-fit of Eq. (1) to the data, we remain with Eq. (3). In fact, we reduce the distortion of $d(t)^{\mathrm{expm}}$ directly by varying only the physical model parameters $c_1, \ldots, c_M$ in its denominator. This amounts to a search in exclusively

the finite, *physical parameter* space. Recall that the ensuing estimate is free of bias in absence of noise. In practice, this is achieved [9] by feeding $d(t)^{\mathrm{expm}} \equiv d(c_1, \ldots, c_M, t)^{\mathrm{expm}}$ into a highpass filter [14] and minimising the sum of the p-th powers of the absolute values[3] of the filter output at selected time points t_n with a genetic algorithm (GA) named PIKAIA [15], *i.e.*,

$$\min_{\substack{c_1,\ldots,c_M \\ \text{PIKAIA}}} \left(\sum_{n_{\mathrm{selected}}} \left| d(c_1, \ldots, c_M, t_n)^{\mathrm{expm}}_{\mathrm{highpassed}} \right|^p \right), \tag{4}$$

where $d(t_n)^{\mathrm{expm}}_{\mathrm{highpassed}}$ is the output of the mentioned highpass filter and $t_{n_{\mathrm{selected}}}$ are those sample points for which $|s(t_n)| \geq a \times \sigma_{noise}$, in which σ_{noise} is the standard deviation of the measurement noise. a is a typical hyper-parameter, usually in the region of 2.5 – 3.5. When $|s(t_n)| < a \times \sigma_{noise}$, the probability of distorting $d(t)^{\mathrm{expm}}$ is deemed too high. Fig. 3 shows how the selection of sample points takes place.

Until recently, we concentrated on $p = 2$, but preliminary results indicate that $p = 1$ seems to be at least as good.

To accommodate consideration (c) in the paragraph *Physical conditions*, above, the cutoff frequency of the highpass filter was set to $\pm 0.007/\triangle t$. Fig. 4 shows the change of $|d(t)^{\mathrm{expm}}|$ produced by Eq. (4). As for judging the size of the change depicted in the Figure, refer to $|d(t=0)^{\mathrm{expm}}| = 1$.

It should now be realised that the values of $c_1, \ldots, c_M$ resulting from Eq. (4) are already optimal estimates of the physical model parameters [9]. Therefore, continuing the estimation by iterative NLLS-fitting of Eq. (1) including smoothing of distortions of $d(t)^{\mathrm{expm}}$, as done in method 2.**i**, is superfluous. The fact that this alternative **ii** leaves details of the form of $d(t)^{\mathrm{expm}}$ unknown is usually of no concern to clinicians.

This ends the parameter estimation procedure indicated by method 2. (More in Sec. IV-C.)

The present work is based on alternative 2**ii**.

III. Results

A. *Method 1. Exponential decay*

Fig. 2 shows the results of fitting the model function of Eq. (1) using exponential decay, $d_m(t) = e^{\alpha_m t}$, $\alpha_m < 0$ to a signal simulated with Eq. (1) using $d_m(t) = d(t) = e^{\alpha t + \beta t^2}, \alpha, \beta < 0$, and adding Gaussian noise. As expected, the residue contains not only random noise, but also the parts of the signal that do not decay exponentially. As a result, the estimates of the concentrations c_m became biased. At high SNR, upper left in Fig. 2, the residue of each of the four big singlets can be seen to contain a doublet. This doublet originates from the difference between exponential and Gaussian decay. With decreasing SNR, the doublets gradually disappeared into the random noise. One wonders at which random noise level the bias in a concentration c_m is superseded by the random error. This question is answered by the numbers in Table. I.

[3] **NB.** Taking the absolute value enables ignoring an overall phase and an overall frequency-shift in the denominator of Eq. (3).

Table I
MONTE CARLO ESTIMATION RESULTS WITH 1000 NOISE REALISATIONS FOR THE CONCENTRATIONS c_m OF METABOLITES $m = 1, \ldots, 5$, FOR SEVEN LEVELS OF THE NOISE, IN ARBITRARY UNITS. A CONVENIENT, EXPONENTIAL DECAY FUNCTION WAS USED. BESIDES THE MEAN OF THE CONCENTRATION (AMPLITUDE) ESTIMATES, THE CORRESPONDING TRUE VALUES $c_m(\mathrm{true})$ ARE ALSO LISTED.

Error	← NOISE LEVEL (a.u.) →						
-	×0†	×1	×2	×3	×4	×5	×6
-	$m = 1$, Choline. $c_1(\mathrm{true}) = 144.0$						
mean	146.78	146.74	146.71	146.69	146.66	146.80	146.03
bias	2.78	2.74	2.71	2.69	2.66	2.80	2.03
sd	N.A.	0.91	1.81	2.72	3.62	4.58	5.67
bias/sd	N.A.	3.02	1.50	0.99	0.73	0.61	0.36
RMSE	2.78	2.89	3.26	3.82	4.50	5.37	6.02
-	$m = 2$, Creatine. $c_2(\mathrm{true}) = 544.0$						
mean	575.17	575.25	575.36	575.47	575.61	574.10	571.19
bias	31.17	31.25	31.36	31.47	31.61	30.10	27.19
sd	N.A.	2.31	4.62	6.92	9.24	11.68	14.52
bias/sd	N.A.	13.54	6.79	4.55	3.42	2.58	1.87
RMSE	31.17	31.34	31.69	32.23	32.93	32.28	30.83
-	$m = 3$, Glutamate. $c_3(\mathrm{true}) = 280.0$						
mean	256.13	256.15	256.07	255.91	255.66	256.41	252.31
bias	-23.87	-23.85	-23.93	-24.09	-24.34	-23.59	-27.69
sd	N.A.	4.07	8.14	12.20	16.24	20.74	25.51
bias/sd	N.A.	-5.85	-2.94	-1.97	-1.50	-1.14	-1.09
RMSE	23.87	24.19	25.27	27.01	29.26	31.42	37.65
-	$m = 4$, Myo inositol $c_4(\mathrm{true}) = 118.0$						
mean	107.13	107.03	106.91	106.78	106.64	106.78	108.67
bias	-10.87	-10.97	-11.09	-11.22	-11.36	-11.22	-9.33
sd	N.A.	2.04	4.08	6.13	8.19	10.38	12.88
bias/sd	N.A.	-5.37	-2.72	-1.83	-1.39	-1.08	-0.72
RMSE	10.87	11.16	11.82	12.78	14.00	15.29	15.91
-	$m = 5$, N-Acetylaspartate. $c_5(\mathrm{true}) = 394.0$						
mean	419.00	419.05	419.12	419.21	419.33	418.31	416.84
bias	25.00	25.05	25.12	25.21	25.33	24.31	22.84
sd	N.A.	2.53	5.06	7.60	10.15	12.96	15.80
bias/sd	N.A.	9.89	4.96	3.32	2.50	1.88	1.45
RMSE	25.00	25.17	25.63	26.34	27.28	27.55	27.77

† At noise level is zero, the standard deviation (sd) is zero. At the same time, the ratio bias/sd is undefined. Hence 'N.A.' — not applicable — in this column.

Table I shows the Monte Carlo results of the concentrations c_m for model function fitting with exponential decay, at seven different noise levels equalling those of Fig. 2 (except ×0 which is not included there).

In absence of noise, see column ×0, the notion of standard deviation does not apply (N.A.), while the bias is significant, due to incorrectly assuming exponential decay. As noise increases, from left to right in the Table, the standard deviation (sd) gradually becomes significant too. However, the noise level where bias and sd cross over, differs per metabolite.

B. *Method 2. Experimental decay*

Following Sec.II-C, point 1, an incorrect but analytic model function, namely Eq. (1) with $d_m(t) = e^{\alpha_m t}$, was first fitted to the signal, merely to obtain starting values of the physical

Table II
MONTE CARLO ESTIMATION RESULTS WITH 1000 NOISE REALISATIONS FOR THE CONCENTRATIONS c_m OF METABOLITES $m = 1, \ldots, 5$, FOR SEVEN LEVELS OF THE NOISE, IN ARBITRARY UNITS. METHOD 2 WAS USED, *i.e.*, NO SURROGATE DECAY FUNCTION. BESIDES THE MEAN OF THE CONCENTRATION (AMPLITUDE) ESTIMATES, THE CORRESPONDING STARTING VALUES $c_m(\text{start})$ AND TRUE VALUES $c_m(\text{true})$ ARE ALSO LISTED. THE POWER p IN EQ. (4) WAS 2.

Error	← NOISE LEVEL (a.u.)→						
-	$\times 0^{\dagger}$	$\times 1$	$\times 2$	$\times 3$	$\times 4$	$\times 5$	$\times 6$
-	$m = 1$, Choline. $c_1(\text{start}) = 147.0$, $c_1(\text{true}) = 144.0$						
mean	144.00	144.11	144.64	145.49	146.73	148.50	151.38
bias	0.00	0.11	0.64	1.49	2.73	4.50	7.38
sd	N.A.	1.18	2.40	3.67	5.07	6.42	8.01
bias/sd	N.A.	0.10	0.27	0.41	0.54	0.70	0.92
RMSE	0.00	1.18	2.49	3.96	5.76	7.84	10.89
-	$m = 2$, Creatine. $c_2(\text{start}) = 576.0$, $c_2(\text{true}) = 544.0$						
mean	544.04	543.76	540.87	538.07	533.78	527.48	519.59
bias	0.04	-0.24	-3.13	-5.93	-10.22	-16.52	-24.41
sd	N.A.	3.89	7.69	11.47	15.85	20.28	24.97
bias/sd	N.A.	-0.06	-0.41	-0.52	-0.64	-0.81	-0.98
RMSE	0.00	3.90	8.31	12.92	18.85	26.16	34.92
-	$m = 3$, Glutamate. $c_3(\text{start}) = 255.0$, $c_3(\text{true}) = 280.0$						
mean	279.99	280.83	278.50	274.15	267.20	260.81	259.86
bias	-0.01	0.83	-1.50	-5.85	-12.80	-19.19	-20.14
sd	N.A.	4.86	9.59	14.59	20.02	26.02	31.24
bias/sd	N.A.	0.17	-0.16	-0.40	-0.64	-0.74	-0.64
RMSE	0.00	4.93	9.71	15.72	23.76	32.33	37.17
-	$m = 4$, Myo inositol. $c_4(\text{start}) = 107.0$, $c_4(\text{true}) = 118.0$						
mean	117.99	118.24	120.23	122.56	126.81	132.67	135.15
bias	-0.01	0.24	2.23	4.56	8.81	14.67	17.15
sd	N.A.	2.62	5.27	7.70	10.10	13.05	16.67
bias/sd	N.A.	0.09	0.42	0.59	0.87	1.12	1.03
RMSE	0.00	2.63	5.72	8.95	13.40	19.63	23.91
-	$m = 5$, N-Acetylaspartate. $c_5(\text{start}) = 420.0$, $c_5(\text{true}) = 394.0$						
mean	393.98	393.17	394.45	395.65	397.74	398.77	397.99
bias	-0.02	-0.83	0.45	1.65	3.74	4.77	3.99
sd	N.A.	3.29	6.57	10.13	13.47	16.62	19.56
bias/sd	N.A.	-0.25	0.07	0.16	0.28	0.29	0.20
RMSE	0.00	3.40	6.59	10.26	13.98	17.29	19.97

† At noise level is zero, the standard deviation (sd) is zero. At the same time, the ratio bias/sd is undefined. Hence 'N.A.' — not applicable — in this column.

parameters. Substitution of these starting values into Eq. (3) yielded a distorted version of the decay. As treated above, most of the distortions were separated from the rest with a highpass filter, and then minimised by searching in the physical parameter space with a Genetic Algorithm (GA). See [9] for details of the GA. Minimal distortion coincided with optimality of physical model parameters.

Table II shows the Monte Carlo results of the concentrations c_m obtained by minimising the mentioned distortions, at seven different noise levels equalling those of Fig. 2 (except $\times 0$ which is not included there). As expected, the method can indeed estimate accurate concentrations, *i.e.*, bias ≈ 0, without using either a correct analytical model function of the decay or a search in function space, provided that noise is absent; see column $\times 0$. With the given levels of noise, the bias/sd ratio remains below 1, except for metabolite 4, columns 6 and 7, row 4.

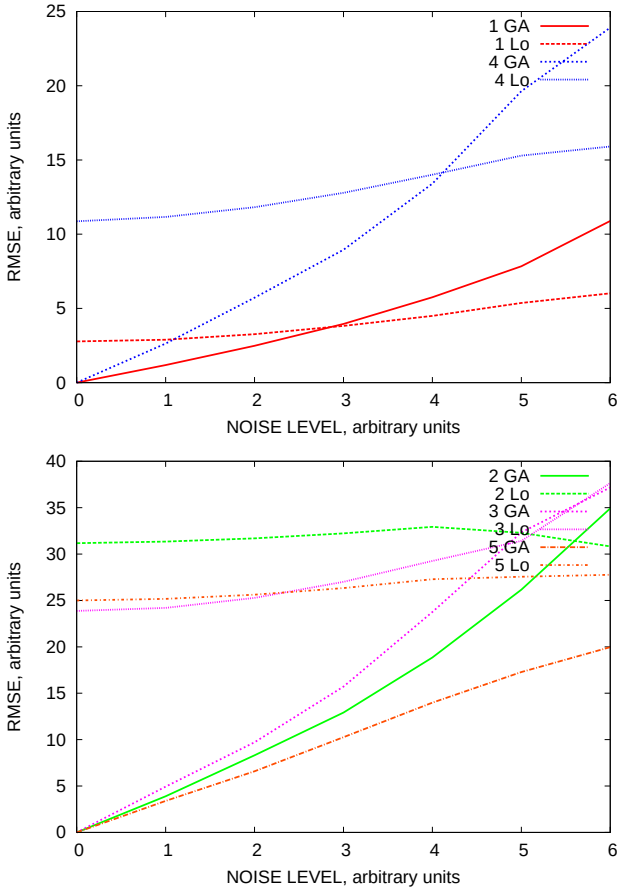


Figure 5. Root mean square errors (RMSE) of the metabolite concentrations in the two methods in this report for seven levels of the SNR (Noise $\times 0, \times 1, \times 2, \times 3, \times 4, \times 5, \times 6$). 1GA = metabolite 1, Genetic Algorithm (PIKAIA). 1Lo = metabolite 1, Lorentz (exponential decay), and similar for metabolites 2,3,4,5.

C. *Root mean square errors*

Fig. 5 shows the root mean square errors = $\sqrt{\text{bias}^2 + \text{sd}^2}$ (RMSE) obtained with the two methods, again for the same seven levels of noise. To avoid crowding, the five metabolites were separated into two groups, metabolites 1,4, and metabolites 2,3,5, as was done in Fig. 1.

As expected, the RMSE incurred by method 1 is already significant at zero noise; but less so for metabolites 1,4 (upper figure) than for metabolites 2,3,5 (lower figure). Method 2, on the other hand, is very accurate at zero noise, for all five metabolites.

Clearly, the RMSE's of method 1 increase slower with increasing noise than do those of method 2. In fact, for metabolite 1, the RMSE's of the two methods become equal at noise level $\times 3$. For metabolite 4, this happens at noise level $\times 4$. For the remaining metabolites equality of RMSE's happens at noise level $\times 5$ or higher.

IV. Discussion

A. *Rationale of the work*

This report concerns bias-variance trade-off. Bias is unavoidable in semi-parametric estimation, *i.e.*, when the model function to be fitted to the data is partly unknown. Here, the unknown part of the model function is the decay of an *in vivo* MRS-signal. Possible other parts in an *in vivo* MRS-signal that lack a model function are contributions from water and macromolecules [16]. The latter two are ignored in this report.

A fundamental problem of dealing with real-world signals is that bias and variance cannot be estimated separately. Consequently, real-world signals are unfit for studying bias-variance trade-off.

A partial judgement of estimation quality can be obtained from analysing the residue of a model fit to a signal. However, possible correlation between physical model parameters and surrogate model parameters can make the presence of bias in the residue invisible. For this reason we worked with a simulated signal of which all was known by definition. Bias and variance could be separated via a Monte Carlo procedure, *i.e.*, using a great number of noise realisations, each added to a noiseless simulated signal, resulting in as many noisy versions of one and the same noiseless signal.

Knowledge of the bias-variance ratio enables one to judge whether use of a convenient, efficient, surrogate model function is justified at a given SNR. The aim is to gain insight that can be used with clinical, typically once-only measurements.

B. *High SNR*

Manufacterers increase the field-strength of new scanners continually. Already, a whole-body MRI/MRS scanner with $B \geq 11$ Tesla has been delivered.[4] Signals from such scanners will have high SNR [16] and the decay will be dominated by micro-susceptibility [5]. Due to the latter of the two properties, the form of the decay will be *a priori* unknown. Consequently, methods 2**i** and 2**ii**, described in Sec. II-C, will become useful in the near future.

An extra feature of method 2**ii** is that, in absence of noise, it estimates concentrations of metabolites without bias (and of course without random error). As explained in Sec. II-C, this is achieved by searching in the physical parameter space only. In other words, even though a correct physical model function lacks, the usual search in function space with attendant bias is avoided.

As for method 1, at high SNR and high magnetic field, it suffers from high bias-to-sd ratio.

C. *Intermediate SNR*

At intermediate SNR, the noise-enhancing mechanism of the division in Eq. (3) requires countermeasures. These measures are treated already in [8], [9], [12] and references therein. But more is needed, especially for extending the applicability of Eq. (3) to ever lower SNR.

So far, our efforts were concentrated on reducing the 'spiky', distorted noise resulting from the division in Eq. (3). However, as mentioned in Sec. II-C, we have come to realise that it could be worthwhile to reduce the noise in the *numerator* of Eq. (3) first, *i.e.*, prior to executing the division. The reasoning behind this is that prior to division, the distribution of the noise is Gaussian, whereas this property is lost during division. Gaussian noise should be more manageable than non-Gaussian, 'spiky', distorted noise[5].

For noise-reduction, we chose the State-Space based method HSVD. Note that the samples of $s(t)$ processed by HSVD were the same as those used in the division; no more, no fewer.

As most methods, HSVD involves setting a hyper-parameter, namely the number of sinusoids used for reconstructing the signal. Setting hyper-parameters is a nuisance for both developers and users. Here, the complication is due to non-exponentiality of the decay, so that each sinusoid needs in principle an infinite number of singular values for perfect reconstruction; in practice, the number depends on the SNR too. To reduce possible sensitivity to hyper-parameter choice, we set the number of sinusoids consecutively to $40, 41, \ldots, 55$ and used the median of the resulting sixteen reconstructions.

More research on noise reduction prior to executing Eq. (3) is necessary[6]. So far, our noise reduction prior to Eq. (3) amounts to about 30%.

Fig. 3 shows how time points t_n at which $|s(t_n)| = a \times \sigma_{noise}$ where a is in the region 2.5 - 3.5, can be identified. These time points are excluded from the minimisation procedure of Eq.(4). The change of $|d(t_n)^{\mathrm{expm}}_{\mathrm{highpassed}}|$, brought about by the minimisation procedure, in absence and presence of noise is shown in Fig. 4.

The red curve, pertains to the noiseless case. Hence, it corresponds to the changing the parameters $c_1, \ldots, c_M$, from the starting values to the final, true values. In simulations, such a curve can serve as 'gold standard' for judging a curve depicting the change for a noisy case.

Turning then to the blue curve (noisy case) in Fig. 4, note first that it contains surprisingly little noise. To understand this, it must be realised that only the noiseless part of Eq. (3) is sensitive to small changes of $c_1, \ldots, c_M$, whereas the noisy part is almost invariant under such small changes. As a result, the graph of the *subtraction* $\left(\left|d(t_n)^{\mathrm{expm,post_pikaia}}_{\mathrm{highpassed}}\right| - \left|d(t_n)^{\mathrm{expm,pre_pikaia}}_{\mathrm{highpassed}}\right|\right)$ shows only minor noisy features. The Figure in the Appendix shows the high level of noise distortion prior to subtraction.

The modest level of the noise in the blue curve of Fig. 4 explains the success of Eq. (4) seen in Table II. Nonetheless, omission of sensitive time points t_n remained necessary. Without it, the MRSEs are higher. In fact, the difference between the blue and red curves in some regions constitutes a reminder that the detrimental effect of noise — random (zero-mean) and systematic (bias) — is inevitable. So far, the mechanism causing the bias quoted in Table II is elusive.

Another matter requiring more research is the setting of

[4] In the present study B is only 3 Tesla, for practical reasons. Simulations at $B \geq 11$ Tesla are envisioned.

[5] So far, we were unable to exploit the fact that the spike-producing mechanism is analytically known.

[6] Application of Cadzow's method [17], [18], [19], [20] is envisioned too.

the highpass filter that separates most of the distortions of $d(t)^{\text{expm}}$ from the rest.[7] In [9], the cutoff frequency of the highpass filter was $\pm 0.05/\triangle t$. At the time, we reported that this value was not critical, which still holds. However, in the light of extending the range of manageable SNR's downward as far as possible, we lowered the cutoff frequency to $\pm 0.007/\triangle t$.

An aspect continually under consideration is how best to deal with a once-only clinical measurement. The fact that method 2 needs an initial round of method 1, implies that it is not difficult how to begin. Depending on the SNR, visible structure in the FFT of the ensuing residue reveals the situation. For example, the upper left picture in Fig. 2 shows that the residue of each of the four intense singlets is a similar-looking doublet. This is indicative of equal non-exponential decay of each sinusoid in the signal. Clearly, continuing as method 2 is then in order. However, Fig. 2 shows too that this pattern of the residue disappears gradually with decreasing SNR and that it is hard to decide at which SNR it is really gone. The results in Fig. 5 complicate the situation even more: The SNR at which the RMSE of method 2 is lower than that of method 1, depends on the metabolite. Therefore it is not yet possible to automate a decision in the clinic as to which method to use at a given SNR.

D. *Low SNR*

Low SNR will never go away. This is a sad fact. However, low SNR justifies use of the simple method 1: Bias due to lack of knowledge about the model function is overshadowed by the random estimation error. At high field, one can then reduce the latter by imposing that all exponential decay parameters $\alpha_m, m = 1, \ldots, M$ be equal, with little or no effect on the bias.

V. Concluding Remarks

1) Clinics move to ever higher magnetic field, benefiting from the overwhelming advantage of high SNR. Another high-field feature is that *in vivo* micro-susceptibility effects dominate the decay of the MRS-signal. Although the form of the resulting decay is *a priori* unknown, it seems reasonable to assume that it does not depend on metabolite-species. This property turns out to be an important asset.
2) We show that an *a priori* unknown form of the decay need not prevent accurate quantitation of metabolites. In fact, in absence of noise, the bias is zero.
3) The vanishing bias mentioned in point 2) can be achieved by using an experimental model function of the decay that becomes correct once its physical model parameters have attained correct values (genetic algorithm).
4) Use of a surrogate analytic model function of the decay, although computationally convenient, can cause significant bias.
5) At low SNR, the random error in the estimated metabolite concentrations is high and exceeds bias with both methods. In this case, choosing a convenient surrogate analytic decay function is obvious.
6) At intermediate SNR, bias-variance trade-off is important. A choice between experimental decay and surrogate analytic decay is to be made for every case. Automation of the choice has not yet been achieved.

[7] This pertains to consideration (c) in the paragraph *Physical conditions* of Sec. II-C.

Acknowledgement

This work is an aftermath of the EU Marie Curie Research Network, FAST, MRTNCT-2006-035801.
Etc.

References

[1] K. Pinker, A. Stadlbauer, W. Bogner, S. Gruber, and TH. Helbich, "Molecular imaging of cancer: MR spectroscopy and beyond," *European Journal of Radiology*, vol. 81, pp. 566–577, 2012. 1

[2] C.H. Kim, A.R. Mijar, and J.S. Arora, "Development of simplified models for design and optimization of automotive structures for crashworthiness," *Struct Multidisc Optim*, vol. 22, pp. 307–321, 2001. 1

[3] P.J. Bickel, C.A.J. Klaassen, Y. Ritov, and J.A. Wellner, *Efficient and Adaptive Estimation for Semiparametric Models*. Springer, paperback 1998. 1

[4] M.R. Kosorok, "What's so Special about Semiparametric Methods?" *The Indian Journal of Statistics*, vol. 71-A, Part 2, pp. 331–353, 2009. 1

[5] D.K. Deelchand, P-F. Van de Moortele, G. Adriany, I. Iltis, P. Andersen, J.P. Strupp, J.P. Vaughan, K. Uğurbil, and P-G. Henry, "*In vivo* ^{1}H NMR spectroscopy of the human brain at 9.4 T: Initial results," *Journal of Magnetic Resonance*, vol. 206, pp. 74–80, 2010. 1, 2, 7

[6] P. van Gelderen, J.A. de Zwart, J. Lee, P. Sati, D.S. Reich, and J.H. Duyn, "Nonexponential $T_2^\star$ decay in white matter," *Magnetic Resonance in Medicine*, vol. 67, pp. 110–117, 2012. 1

[7] D. Stefan, F. Di Cesare, A. Andrasescu, E. Popa, A. Lazariev, E. Vescovo, O. Strbak, S. Williams, Z. Starcuk, M. Cabanas, D. van Ormondt, and D. Graveron-Demilly, "Quantitation of magnetic resonance spectroscopy signals: the jMRUI software package," *Meas. Sci. Technol.*, vol. 20, 2009, http://www.mendeley.com/research/quantitation-magnetic-resonance-spectroscopy-signals-jmrui-software-package/. 1, 2

[8] E. Popa, D.A. Karras, B.G. Mertzios, D.M. Sima, R. de Beer anda D. van Ormondt, and D. Graveron-Demilly, "Handling unknown lineshape without searching in function space. Application to in vivo metabolite quantitation." *Meas. Sci. Technol.*, vol. 22, 2011, http://iopscience.iop.org/0957-0233/22/11/114014. 1, 2, 4, 7

[9] D. van Ormondt, R. de Beer, D.M. Sima, and D. Graveron-Demilly, "New Approach to Semi-Parametric Estimation for *In Vivo* Magnetic Resonance Spectroscopy," in *ProRISC, ICT.OPEN*. Veldhoven, The Netherlands: IPN, STW, NWO, 27-28 November 2011, pp. 45–50, http://www.ictopen2012.nl/files.nsf/pages/NWOP_8U5FRX/$file/Ormondt_D.pdf. 1, 2, 4, 5, 6, 7, 8

[10] D. Graveron-Demilly, A. Diop, A. Briguet, and B. Fenet, "Product-operator algebra for strongly coupled spin systems," *Journal of Magnetic Resonance*, vol. A101, pp. 233–239, 1993. 2

[11] A. van den Bos, *Parameter Estimation for Scientists and Engineers*. Wiley, 2007. 2

[12] M.I. Osorio-Garcia, D.M. Sima, F.U. Nielsen, T. Dresselears, F. Van Leuven, U. Himmelreich, and S. Van Huffel, "Quantification of in vivo ^{1}H Magnetic Resonance Spectroscopy (MRS) signals with baseline and lineshape estimation ," *Meas. Sci. Technol.*, vol. 22, 2011, http://iopscience.iop.org/0957-0233/22/11/114011. 4, 7

[13] R. de Beer and D. van Ormondt, *in: NMR Basic Principles and Progress*. Springer, 1992, vol. 26, ch. 'Analyis of NMR data using Time-Domain Fitting Procedures', pp. 201–248. 4

[14] P.B. Pynsent and R. Hanka, "A simple program for a phaseless recursive digital filter," *Journal of Biomedical Engineering*, vol. 4, no. 3, pp. 252–254, July 1982, doi:10.1016/0141-5425(82)90011-5. 5

[15] P. Charbonneau and B. Knapp, *A User's Guide to PIKAIA 1.0, NCAR/TN-418+IA, NCAR Technical Note*, High Altitude Observatory National Center For Atmospheric Research Boulder, Colorado, Deecember 1995, http://www.hao.ucar.edu/modeling/pikaia/pikaia.php. 5

[16] R.A. de Graaf, *In Vivo NMR Spectroscopy: Principles and Techniques*, 2nd ed. Wiley, 2007. 7
[17] J.A. Cadzow, "Signal enhancement - A composite property mapping algorithm," *IEEE Trans. Acoust., Speech., Sig. Proc.*, vol. 36, pp. 49–62, 1988. 7
[18] A. Diop, A. Briguet, and D. Graveron-Demilly, "Automatic in vivo nmr data processing based on an enhancement procedure and linear prediction method," *Magn. Reson. Med.*, vol. 27, pp. 318–328, 1992. 7
[19] A. Diop, Y. Zaim-Wadghiri, A. Briguet, and D. Graveron-Demilly, "Improvements of quantitation by using the Cadzow enhancement procedure prior to any linear-prediction methods," *J. Magn. Reson.*, vol. B 105, pp. 17–24, 1994. 7
[20] H.S. Taylor, A. Kershaw, and R. Haiges, "Handbook Algorithm for the Denoising 1D NMR For Obtaining Chemical Shifts With Fewer Transients — More Sensitivity Magnet Resonance Analysis by both Singular Value Decomposition Harmonic Inversion and Stability and Phase Criteria for Distinguishing Signal from Noise," University of Southern California, Tech. Rep., 2009, 31 pp. 7

2012-08-08 11:39

VI. Appendix

See Fig. 6 on page 10. The grey and black (dotted) lines indicate regions of $t_{n_{\text{selected}}}$ excluded from minimisation according to Eq. (4). In an excluded region a straight line is drawn connecting the values of the nearest points in the adjacent included regions. Without this measure, outliers dominate the graphs.

a. Similar to Fig. 3, yet included for better overview. The noise in $s(t_n)$, prior to noise reduction with HSVD, is as shown in Fig. 2, 'Noise $\times 3$'.

b. Comparison of $d(t_n)^{\text{expm,post_pikaia}}$ (blue) with its lowpassed version (red).

c. The real-valued (blue) and imaginary-valued (red) parts of $d(t_n)^{\text{expm,pre_pikaia}}_{\text{highpassed}}$, *i.e.*, prior to Eq. (4).

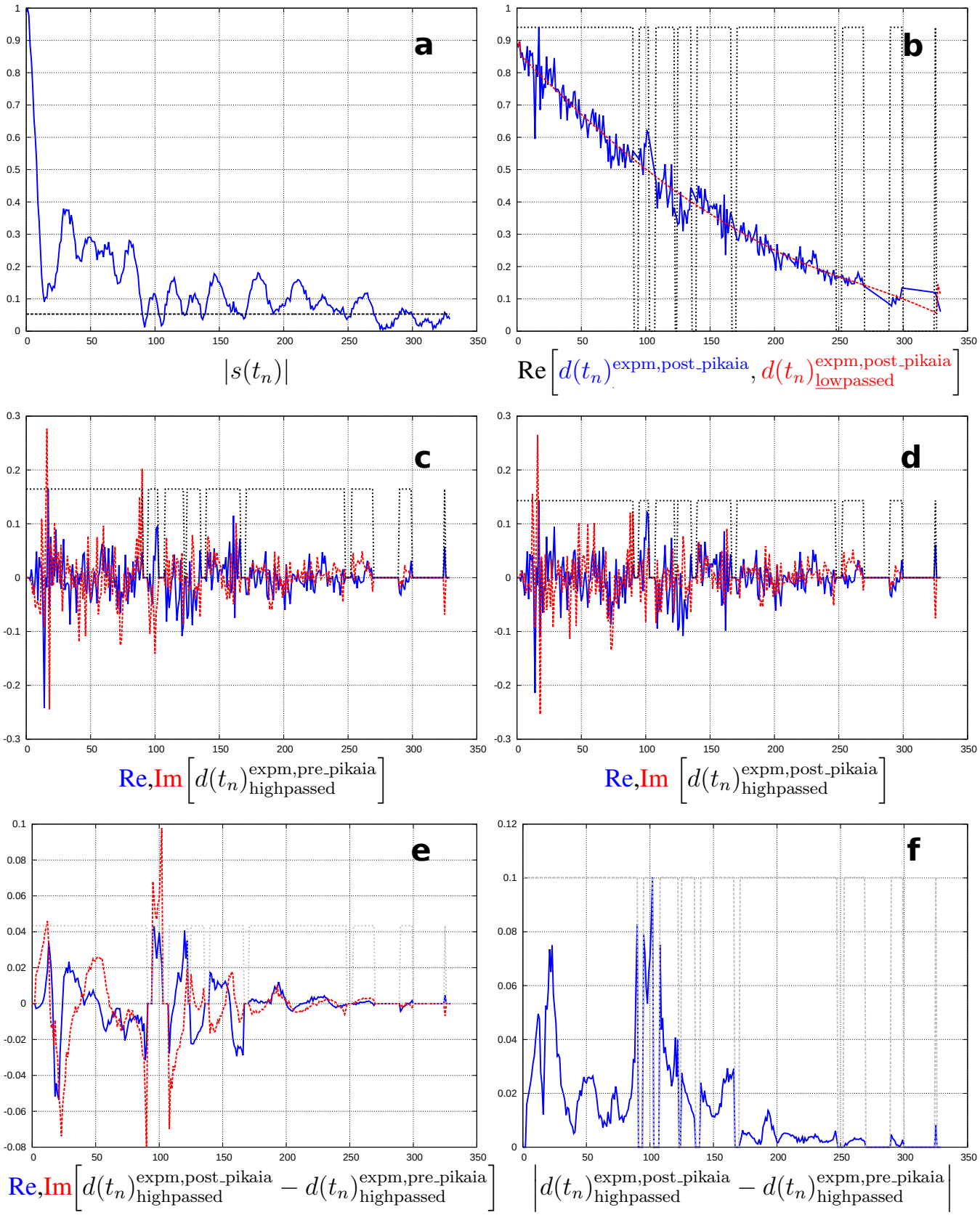
d. The real-valued (blue) and imaginary-valued (red) parts of $d(t_n)^{\text{expm,post_pikaia}}_{\text{highpassed}}$, *i.e.*, after Eq. (4).

Both highpass-filter outputs are very noisy so that distortion due to incorrectness of the values of $c_1, \ldots, c_M$ is hard to distinguish from that due to noise.

However:

e. The graph of the *difference* of the two highpass-filter outputs of **c** and **d** is almost free of noise-related distortion.

f. The absolute value of the difference of **c** and **d**, *i.e.*, $\left| d(t_n)^{\text{expm,post_pikaia}}_{\text{highpassed}} - \; d(t_n)^{\text{expm,pre_pikaia}}_{\text{highpassed}} \right|$, is even more amenable to viewing the distortion due to a change of the values of $c_1, \ldots, c_M$, separated from most of the noise-related distortion.



NB: lowpassed $\stackrel{\mathrm{def}}{=}$ 1 - highpassed.

Figure 6. See the text in the Appendix, page 9. Horizontal axis: t_n in units of $\triangle t$.